

theory. In this way, one obtains

$$\Psi(^5P) = 0.995\Psi(d^5\ ^6S\ p^5P) - 0.101\Psi(d^5\ ^4P\ p^5P) - 0.110\Psi(d^5\ ^4D\ p^5P).$$

Using this function one finds

$$\langle ^7P_3 | \mathcal{H}_{\text{so}} | ^5P_3 \rangle = 0.995 \left(\frac{1}{3}\sqrt{5}\right) \zeta_p + 0.1(10/3)^{1/2} \zeta_a,$$

$$\langle ^7P_2 | \mathcal{H}_{\text{so}} | ^5P_2 \rangle = 0.995 \left(\frac{1}{3}\sqrt{\frac{7}{2}}\right) \zeta_p + 0.1 \left(\frac{1}{3}\sqrt{21}\right) \zeta_a.$$

For ζ_p we may substitute 168 cm⁻¹ and for ζ_a , 250 cm⁻¹.¹⁴ The coefficient of the quintet state admixed to the septet is then simply this matrix element divided by the energy separation and is given in Eqs. (14).

Elastic Differential Scattering of He⁺ Ions by Ne and Ar and of Ar⁺ Ions by Ar in the 10–600-eV Range*

WILLIAM ABERTH AND DONALD C. LORENTS
Stanford Research Institute, Menlo Park, California
(Received 5 November 1965)

Absolute elastic differential scattering cross sections of He⁺ on Ne and Ar and of Ar⁺ on Ar have been measured at relative energies ranging from 10 to 600 eV and scattering angles of 1° to 40°. The He⁺ on Ne and Ar cross sections are monotonically decreasing functions of angle and have a superimposed ripple structure which is attributed to curve-crossing effects. No rainbow-angle structure is evident on these curves. The Ar⁺-on-Ar cross sections indicate both rainbow scattering and oscillations associated with symmetric charge exchange. From the values of the rainbow scattering angle, the estimated binding energy of Ar₂⁺ is 1.6±0.3 eV, assuming the general shape of the attractive potential resembles that of He₂⁺.

I. INTRODUCTION

EXPERIMENTAL and theoretical studies of the differential scattering of He⁺ on He have shown that there is much to be learned about ion-atom interactions from such studies.^{1,2} The He⁺+He elastic interaction was found to be well described by the diabatic ¹Σ_u⁺ and ¹Σ_g⁺ states of He₂⁺. A secondary oscillation found at large angles and energies was identified as a manifestation of nuclear symmetry.³ Another anomaly discovered in the data, a ripple in amplitude of the peaks and valleys, has been attributed to the effect of curve crossing on the elastic scattering.⁴

In this paper we report an experimental study of the differential scattering of He⁺ on Ne and Ar, and of Ar⁺ on Ar. A theoretical analysis of the scattering cross sections has not been attempted, principally because of the lack of computed interaction potentials for these systems. Since only a single ²Σ⁺ state is needed to describe the scattering of He⁺ ions by Ne and Ar, these interactions differ from that of He⁺+He. The Ar⁺+Ar interaction, however, is more complex and requires

perhaps as many as six interaction potentials for its description. This system has recently been studied by Jones *et al.*,⁵ who measured the electron capture probability.

Differential cross sections were measured with the apparatus used for the He⁺+He measurements.¹ Attention was focused on elastic scattering studies although some cursory observations of inelastic scattering are also reported. The He⁺+Ne and He⁺+Ar elastic-scattering cross sections are smooth functions of angle with a slight ripple structure which is attributed to curve crossings. The Ar⁺+Ar elastic scattering is rich in structure because of several different interference processes.

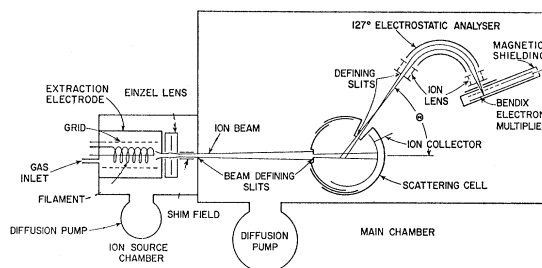


FIG. 1. Schematic diagram of apparatus.

* Supported in part by the Defense Atomic Support Agency through the U. S. Army Research Office (Durham).

¹ D. C. Lorents and W. Aberth, Phys. Rev. **139**, A1017 (1965).

² R. P. Marchi and F. T. Smith, Phys. Rev. **139**, A1025 (1965).

³ W. Aberth, D. C. Lorents, R. P. Marchi, and F. T. Smith, Phys. Rev. Letters **14**, 776 (1965).

⁴ F. T. Smith, D. C. Lorents, W. Aberth, and R. P. Marchi, Phys. Rev. Letters **15**, 742 (1965).

⁵ P. R. Jones, N. W. Eddy, H. P. Gilman, A. K. Jhaveri, and G. Van Dyk, Phys. Rev. (to be published).

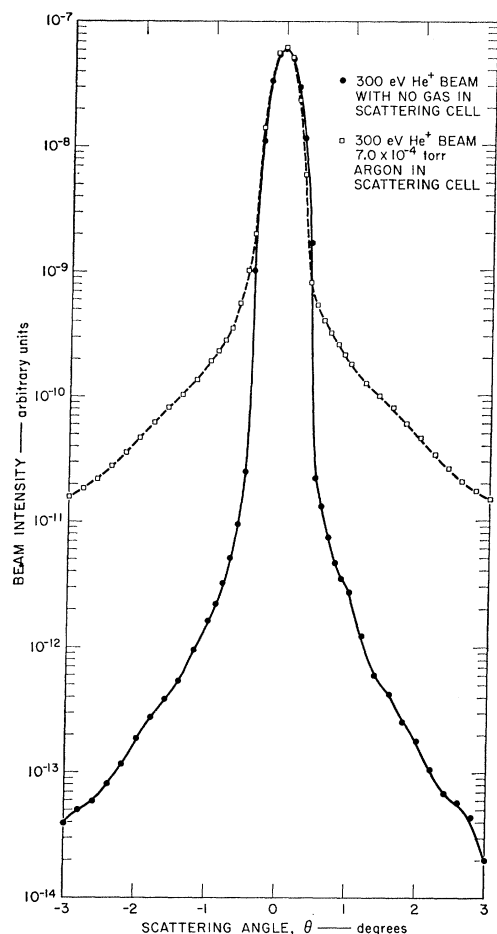


FIG. 2. Beam profile with and without a gas in the scattering cell.

II. APPARATUS AND EXPERIMENTAL PROCEDURE

Since the experimental arrangement and procedure have been described in detail,¹ only a brief description will be given here. A schematic view of the apparatus is shown in Fig. 1. Beam ions are produced in the ion source chamber by a dc electron bombardment discharge maintained between the grid and filament. The ion-gauge pressure reading in the discharge region is kept between 1.5 and 2×10^{-3} Torr for optimum discharge conditions. For an argon beam, the discharge is sustained at a grid potential of 40 V. At this energy the electrons do not possess sufficient energy to produce Ar^{++} or higher metastable states of Ar^+ .⁶ The lower lying $^4D_{7/2}$, $^4F_{9/2}$, $^4F_{7/2}$, and $^2F_{7/2}$ metastable ion states, however, can be produced but should represent only about 1% of the total production of $^2P_{3/2}$ and $^2P_{1/2}$ states of Ar^+ .⁷ The ratio of Ar^+ in the $^2P_{1/2}$ to that in the $^2P_{3/2}$ state is uncertain since there is evidence that it is not produced in statistical equilibrium.⁸ The electron

⁶ J. W. McGowan and L. Kerwin, Can. J. Phys. 41, 1535 (1963).

⁷ H. D. Hagstrum, Phys. Rev. 104, 309 (1956).

⁸ M. Hussain and L. Kerwin, in *Proceedings of the Fourth*

accelerating voltage necessary for a stable helium discharge is 90 eV. The metastable He^+ ($2^2S_{1/2}$) contribution to the beam in comparison to the ground state He^+ ($1^2S_{1/2}$) component is estimated at about 1%,⁹ while the He^{++} contribution is of the order of 0.1%.¹⁰ The contribution of these metastable and doubly ionized components to the scattering signal was well within the experimental error limits and was neglected.

Standard bottled helium, neon, and argon gas, with stated purities of 99.99%, 99.962%, and 99.998%, respectively, were used in the experiment after trapping at dry-ice temperatures.

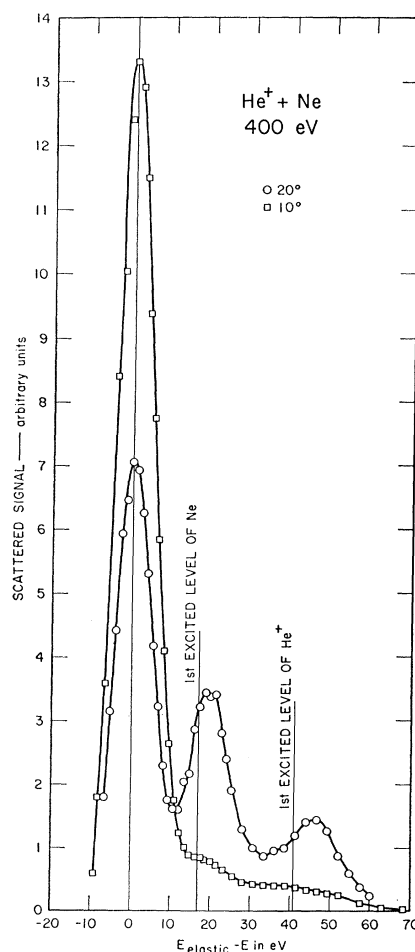


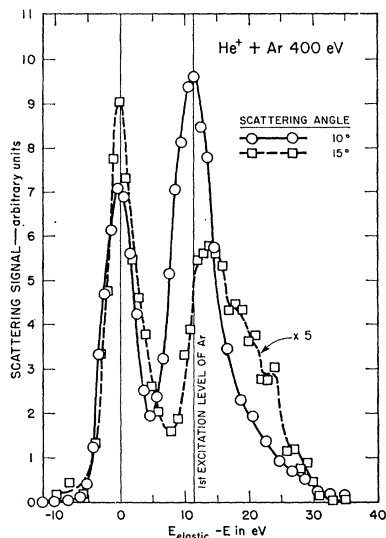
FIG. 3. Energy analysis of 400-eV He^+ ions scattered on Ne at two different scattering angles. The abscissa is the difference between the energy of the elastically scattered ions and the mean energy accepted by the analyzer and to a good approximation equals the excitation energy. Although individual excited states are not resolved, the resolution is sufficient to separate the elastic from the inelastic ions. The relative inelastic component is observed to increase strongly with increasing angle.

International Conference on the Physics of Electronic and Atomic Collisions (Science Bookcrafters, Hastings-on-Hudson, New York, 1965), p. 296.

⁹ W. E. Lamb, Jr., and M. Skinner, Phys. Rev. 78, 539 (1950).

¹⁰ W. Bleakney and L. G. Smith, Phys. Rev. 49, 402 (1936).

FIG. 4. Energy analysis of 400-eV He^+ ions scattered on Ar at 10° and 15° scattering angles. A marked increase in the inelastic component is observed for argon over that of neon (Fig. 3). This large inelastic component effectively limited the maximum energy for resolvable elastic scattering to 400 eV.



The ions, which are extracted from the discharge, are focused by an einzel lens and formed into a collimated beam. All dimensions and spacings of the beam-defining slits are identical with those given in Ref. 1. The ion beam flux that enters the scattering cell varies between 5×10^{-12} A for a 10-eV beam and 2×10^{-8} A for a 600-eV beam. An ion collector, located inside the scattering cell is used to monitor and obtain absolute measurements of the primary ion beam current. An absolute gas pressure of about 8×10^{-4} Torr is maintained in the scattering cell; this is several hundred times higher than the surrounding vacuum pressure (see Fig. 2). This cell pressure is within the region of linear dependence of scattering signal versus scattering gas pressure. The scattered ions leave the cell at an angle defined by a rotatable slit at the cell and the first slit of the 127° electrostatic energy analyzer. In this work an analyzer energy resolution of 4% of the analyzer acceptance energy was attained by decreasing the analyzer exit-slit dimensions to 1.0×0.1 cm. The ions are finally detected by a Bendix M-306-1 magnetic electron multiplier located directly behind the exit slit of the analyzer. The output signal of the multiplier is plotted on a two-pen recorder after further amplification by a Cary 31 vibrating reed electrometer. The second pen of the recorder simultaneously indicates the angular position of the analyzer.

A typical beam profile with and without a gas in the scattering cell is shown in Fig. 2. The half-width of the beam is 0.4° independent of cell pressure. Helium gas which is introduced into the scattering cell by gas leakage from the ion-beam source chamber is the main contributor to the shoulder observed on the beam profile (solid circles in diagram). A faint indication of the He^+ on He interference structure can be observed on this shoulder. The scattering signal produced by the residual gas is less than 1% of the total signal (open circles in diagram) for cell pressures used and con-

stituted a negligibly small error to the measured cross section.

The procedure for obtaining relative differential cross section data and for normalizing the data has already been detailed.¹ In the normalizing procedure, the target-gas pressure was measured by an ion gauge which was calibrated by a McLeod gauge (Scientific Glass Apparatus Co., JV-2490). Some systematic error in the McLeod-gauge reading can be expected from the pumping effect of the mercury vapor.¹¹ Calculations based on the work of deVries and Rol¹² indicate that this effect may cause our measured cross sections in Ne and Ar to be too large by 6% and 13%, respectively. No correction was made for this possible error in the present measurements.

III. DATA AND DISCUSSION

A. Energy Analysis of Scattered Beam

A knowledge of the inelastic-scattering component is essential for two reasons: (1) it is necessary to ascertain that the elastic component is resolved, and (2) the inelastic scattering can influence the elastic scattering. Figures 3, 4, and 5 show some representative energy

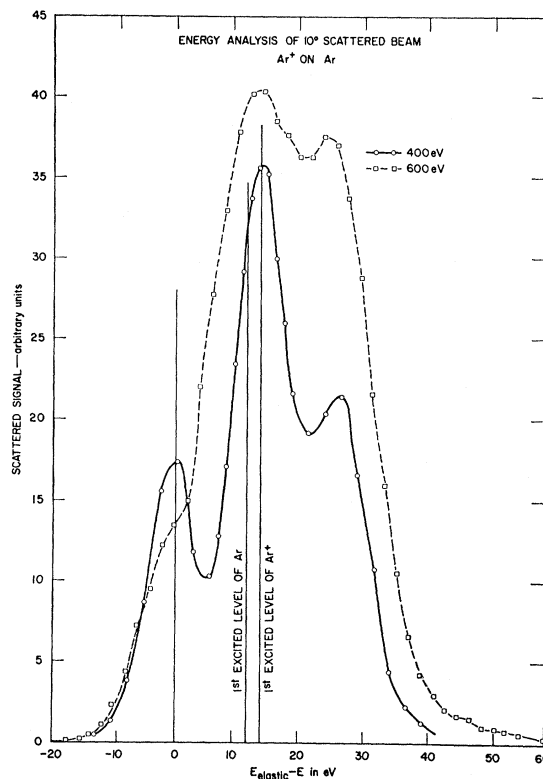


FIG. 5. Energy analysis of 400- and 600-eV Ar^+ ions scattered on Ar at a 10° scattering angle. The decrease in the energy resolution at the higher energy is characteristic of the analyzer.

¹¹ H. Ishii and K. Nakayama, Bull. Electrotech. Lab. (Japan) 25, 657 (1961).

¹² A. E. deVries and P. K. Rol, Vacuum 15, 135 (1965).

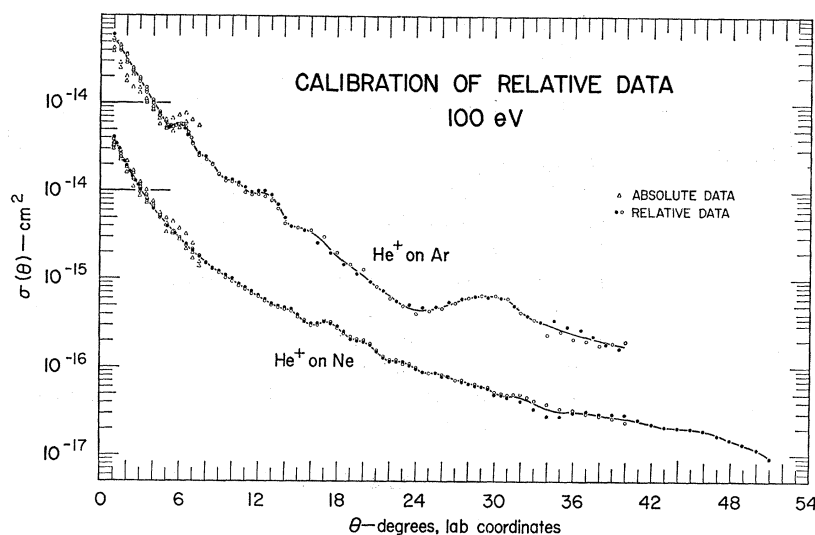


FIG. 6. Exemplary data at 100 eV for He⁺ on Ne and Ar showing data points with an average smooth curve drawn through them. Note the shifted scale; the proper scale is identified at 10^{-14} cm^2 by the intersection of a solid line with each curve. The absolute data points to which the relative data are normalized are also shown.

analyses of the scattered beam. In general, the relative inelastic component tended to increase with increasing scattering angle and incident ion energy. Although the energy resolution of the analyzer was insufficient to resolve collisions producing a particular excited state of the target atom or scattered ion, an interesting structure was observed.

In He⁺ on Ne (Fig. 3) two inelastic peaks occur which have onset energies close to the first excited levels of Ne and He⁺, respectively. A number of auto-ionizing states of neon also occur in the energy range of the second inelastic peak and the excitation of these levels very

likely contributes to this peak.¹³ Only one definite inelastic peak is resolved for He⁺ on Ar (Fig. 4) at energies above 100 eV. Its shape, however, indicates that some of the auto-ionizing levels of argon above 16 eV are contributing to the inelastic scattering.¹³ For this collision the inelastic scattering which results in excitation of the argon atom begins to dominate over elastic scattering at relatively small scattering angles and low incident ion energies. The large amount of inelastic scattering in this collision may explain some of the elastic scattering structure observed for He⁺ on Ar (Sec. IIIC). The Ar⁺-on-Ar energy analysis (Fig. 5)

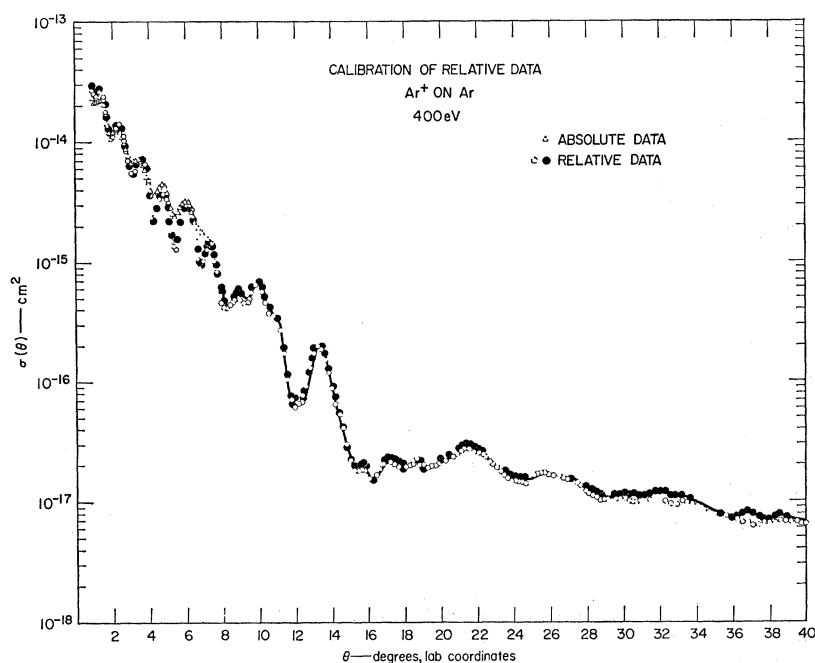


FIG. 7. Exemplary data at 400 eV of Ar⁺ on Ar showing relative data points and the absolute data points to which the relative data are normalized.

¹³ M. E. Rudd and D. V. Lang, in *Proceedings of the Fourth International Conference on the Physics of Electronic and Atomic Collisions* (Science Bookcrafters, Hastings-on-Hudson, New York, 1965), p. 153.

shows an inelastic peak in the vicinity of the first excited levels of both Ar and Ar⁺. The second peak can be interpreted as double excitation of the atom^{13,14} or single excitation of both the atom and the ion. The wider envelope of the 600-eV analysis indicates the decreasing energy resolution of the analyzer rather than a greater spread in the scattered ion energy.

B. Calibration of Relative Data

Figures 6 and 7 show the normalization of the relative cross-section data to the absolute measurements and give an indication of the reproducibility of the data points. It will be noticed that the slopes of the relative curves are somewhat steeper than the absolute curves. This effect is primarily due to two causes. As the scattering angle θ decreases below about 5°, the effect of the analyzer slit height in shifting the true average scattering angle toward larger values becomes important. The slope of the observed cross section therefore decreases below that of the actual cross section as one proceeds toward smaller angles. (A detailed discussion of these effects is given in Ref. 1.) Since the effective slit height is greater in the absolute measurements than in the relative measurements, this distortion is more pronounced for the absolute measurements and the absolute data points tend to fall below the relative points as the angle approaches 0°. As the angle increases beyond 5°, the probability of inelastic scattering can become significant. Since the absolute measurements include inelastic events, they will tend to be greater than the relative measurements which include only elastically scattered ions. At the higher energies where the inelastic effect is important, the absolute curve will therefore cross the relative curve and remain above it at larger angles. The relative data must be matched to the absolute data with proper weight given to both these effects. It is estimated that normalization error is $\pm 20\%$ and the uncertainty in the absolute measurements is $\pm 15\%$. The error bars shown in Fig. 10 for Ar⁺ on Ar represent the reproducibility of the relative data. This reproducibility error is approximately the same for the He⁺ on Ne and Ar data. It is about 10% over most of the angular and energy range but attains a maximum of about 50% at the extreme scattering angles and at the lowest energies. Inelastic contribution to the elastic signal due to insufficient analyzer resolution can be expected at the highest energies (400 to 500 eV and $\theta > 20^\circ$), where the relative inelastic cross section is the largest.

The angular position of the cross section peaks of Ar⁺ on Ar at energies greater than 50 eV was reproducible to within 0.1° for angles less than 8° and to within 0.2° for larger angles. Below 50 eV the repro-

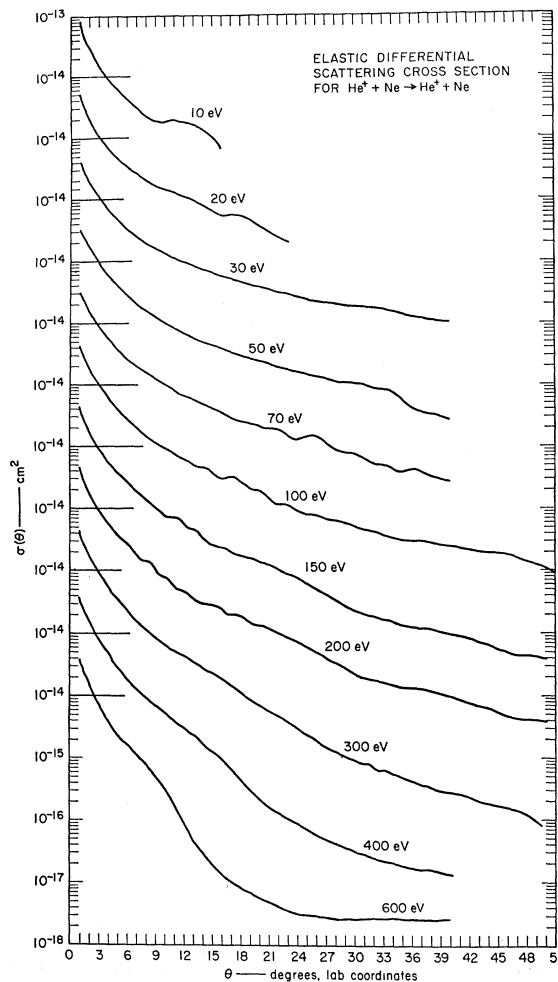


FIG. 8. Elastic differential scattering cross sections for He⁺ on Ne at incident energies from 10 to 600 eV. Note the shifted scale; the proper scale is identified at 10⁻¹⁴ cm² by the intersection of a horizontal line with each curve.

ducibility was about 0.2° for angles less than 5° and 0.4° for larger angles.

C. Elastic Scattering of He⁺ on Ne and Ar

The experimental cross section results of He⁺ on Ne are shown in Fig. 8. The curves show a small-amplitude ripple structure superimposed on a monotonically decreasing cross section. This structure, which is first noticeable at 50 eV, tends to shift with constant $E\theta$, indicating that it is probably associated with a particular region of the potential. This structure we believe to be a perturbation due to a crossing of potential curves in the region of the turning point.⁴ No rainbow scattering is evident in the low-energy data, indicating that the binding energy of the ground $2\Sigma^+$ state of HeNe⁺ is less than a few tenths of an eV. HeNe⁺ has been detected in a gas discharge comprising a mixture of helium

¹⁴ P. R. Jones, T. L. Batra, and H. A. Ranga, in *Proceedings of the Fourth International Conference on the Physics of Electronic and Atomic Collisions* (Science Bookcrafters, Hastings-on-Hudson, New York, 1965), p. 292.

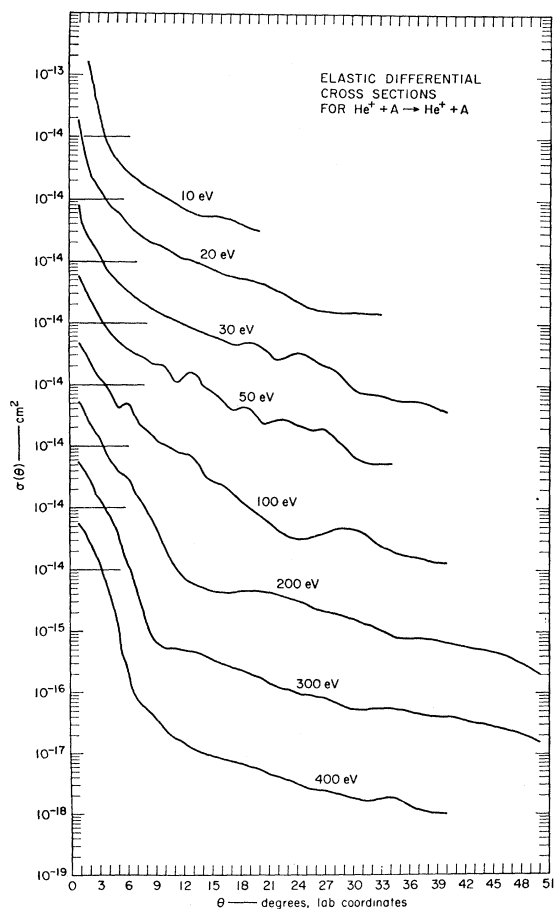


FIG. 9. Elastic differential scattering cross sections for He^+ on Ar at incident energies from 10 to 400 eV. Note the shifted scale; the proper scale is identified at 10^{-14} cm^2 by the intersection of a horizontal line with each curve.

and neon at around 1 Torr, but the state of the HeNe^+ ion has not been identified.¹⁵

The He^+ on Ar cross section structure (Fig. 9) is similar to He^+ on Ne but has some distinguishing characteristics. The ripple structure is present and also tends to move with constant $E\theta$ but has a larger amplitude. Again, no rainbow scattering is observed at low energies. A surprising result at energies above 100 eV is the appearance in the cross section of a very steep initial descent, followed by a rather abrupt leveling off. The very steep initial slope may be partly explained by the rapid increase with angle of inelastic scattering at energies of 200 eV and greater. Inelastically scattered ions remove ions available to the elastic channel and cause a consequent decrease in the elastic scattering signal. The inelastic component eventually dominates the scattering for large angles and energies (Figs. 4 and 5). In the case of He^+ on Ne, the inelastic cross section appears much smaller and the effect is reduced. However, for Ar^+ on Ar (Fig. 10) inelastic scattering is

¹⁵ M. Pahl and U. Weimer, *Naturwiss.* 44, 487 (1957).

dominant at 400 and 600 eV, and a similar decrease is observed on the cross section curves.

D. Ar^+ on Ar

The Ar^+ on Ar data of Fig. 10 show the interference oscillations characteristic of charge exchange scattering by symmetric species.^{1,16} The curves exhibit a more complex nature than He^+ on He. The Ar^+ -on-Ar oscillations are considerably damped at all energies and angles and, furthermore, are highly irregular. This behavior is undoubtedly a reflection of the more complex nature of this system. Since the incident argon ion may exist in either the $^2P_{1/2}$ or $^2P_{3/2}$ ground state, six Ar_2^+ states are possible, namely $^2\Sigma^+_{u,g}$, $^2\Pi_{(u,g)^{3/2}}$, and $^2\Pi_{(u,g)^{1/2}}$.¹⁷ The disappearance of the relatively uniform oscillations at large angles and energies may be due to an increase in interference caused by a greater mixing of the six Ar_2^+

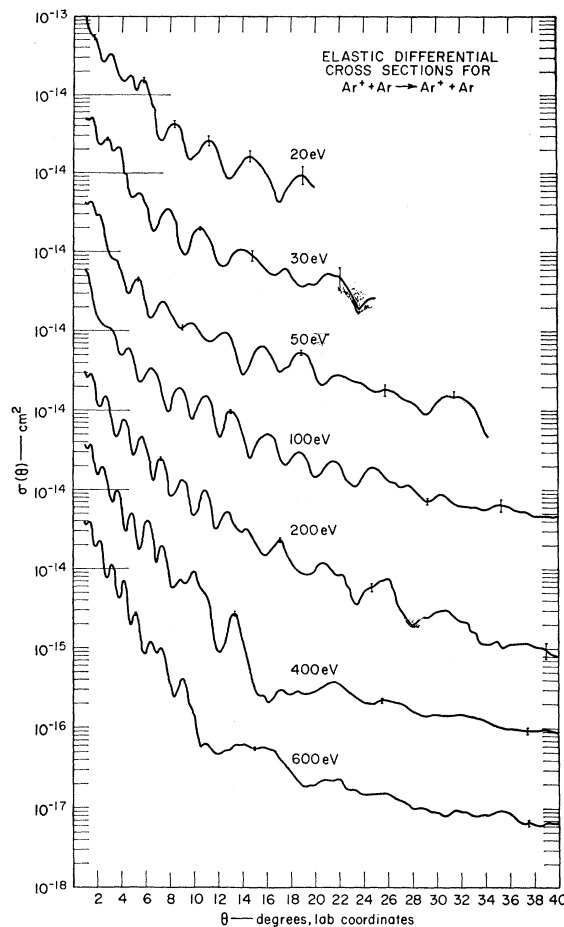
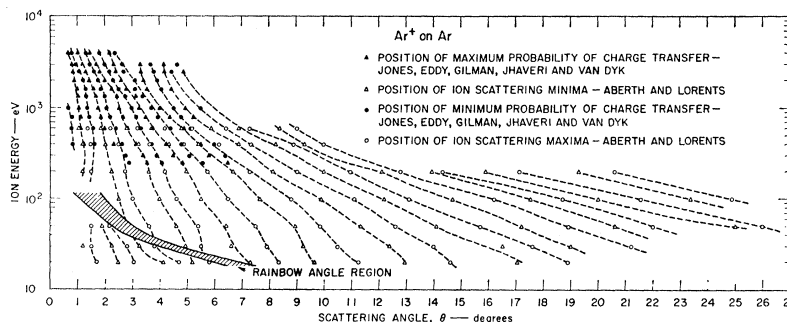


FIG. 10. Elastic differential scattering cross sections for Ar^+ on Ar at incident energies from 20 to 600 eV. Note the shifted scale; the proper scale is identified at 10^{-14} cm^2 by the intersection of a horizontal line with each curve.

¹⁶ H. F. Helbig and E. Everhart, *Phys. Rev.* 140, A715 (1965); P. R. Jones, P. Costigan, and G. Van Dyk, *ibid.* 129, 211 (1963).

¹⁷ R. S. Mulliken, *Phys. Rev.* 136, A962 (1964).

FIG. 11. Map of angular positions of cross-section maxima and minima as a function of energy. Data of Jones, Eddy, Gilman, Jhaveri, and Van Dyk (Ref. 5) are maxima and minima of charge transfer probability.



states at small impact parameters as well as to the increase in inelastic scattering. Nuclear interference³ and curve-crossing effects⁴ in this region should also tend to smear out any regular structure in the cross sections.

As one proceeds toward smaller angles and at energies below 100 eV, an abrupt increase in the cross section is observed which is attributed to rainbow scattering because of its similarity to the identified He^+ on He rainbow scattering.¹ If it is assumed that the shape of the Ar_2^+ potential minimum region is similar to that of He_2^+ , then the value of the Ar_2^+ well depth is approximately equal to $(E\theta_{\text{Ar}}/E\theta_{\text{He}})\epsilon_{\text{He}}$, where $E\theta_{\text{Ar}}$ and $E\theta_{\text{He}}$ represent the values of $E\theta$ at the rainbow angle for Ar_2^+ and He_2^+ , respectively, and ϵ_{He} is the value of the He_2^+ potential minimum. Using the potential of Reagan, Browne, and Matsen,¹⁸ Marchi and Smith² calculated the differential cross section of He^+ on He, and their results are in excellent agreement with the data of Ref. 1, especially in the rainbow angle region. Thus the well minimum of 2.3 eV occurring at about 180 eV deg is reasonably accurate. The value of $E\theta_{\text{Ar}}$ as determined by comparison with the helium data is about 124 eV deg and appears constant. This gives a value for the Ar_2^+ well depth of 1.6 ± 0.3 eV. Cloney, Mason, and Vanderslice¹⁹ have calculated the Ar_2^+ binding energy based on the total cross-section data of Ghosh and Sheridan²⁰ and Cramer.²¹ Their value of 0.056 eV is inconsistent with our results and may be due to their considering only the $^2\Sigma_u$ and $^2\Sigma_g$ electronic states of Ar_2^+ . Evidence of the

existence of Ar_2^+ from mass spectrometry²² and ion-mobility²³ experiments indicate that Ar_2^+ is relatively stable and has a deeper well than that calculated by Cloney *et al.* An accurate description of the potential functions for Ar_2^+ will probably require detailed structure calculations.

Figure 11 gives the positions of maxima and minima of the scattering cross section plotted as a function of energy. The data of Jones, Eddy, Gilman, Jhaveri, and Van Dyk⁵ obtained from measurements of P_0 , the electron capture probability, are also shown. A maximum in the electron capture probability corresponds to a minimum in the ion scattering cross section. Exact agreement of the two sets of data in the region of overlap is not expected since differences of angular resolution and the nature of the quantities measured will cause slight relative shifts of the data points (see Ref. 1). It is interesting to note the appearance and apparent continuation of the ion maxima and minima inside the rainbow region.

ACKNOWLEDGMENTS

We are indebted to Dr. F. T. Smith and Dr. R. P. Marchi for valuable guidance in the interpretation of these results. We also acknowledge many valuable discussions with our colleagues Dr. J. R. Peterson, Dr. O. Heinz, and Dr. C. J. Cook, and we are grateful to the authors of Ref. 5 for use of their data in Fig. 11 prior to publication.

¹⁸ P. N. Reagan, J. C. Browne, and F. A. Matsen, *Phys. Rev.* **132**, 304 (1963).

¹⁹ R. D. Cloney, E. A. Mason, and J. T. Vanderslice, *J. Chem. Phys.* **36**, 1103 (1962).

²⁰ S. N. Ghosh and W. F. Sheridan, *J. Chem. Phys.* **26**, 480 (1957).

²¹ W. H. Cramer, *J. Chem. Phys.* **30**, 641 (1959).

²² J. A. Hornbeck and J. P. Molnar, *Phys. Rev.* **84**, 621 (1951); D. Morris, *Proc. Phys. Soc. (London)* **A68**, 11 (1955); P. F. Knewstubb and A. W. Tickner, *J. Chem. Phys.* **36**, 674 (1962); M. Pahl, *Z. Naturforsch.* **14a**, 239 (1959); P. M. Becker and F. W. Lampe, *J. Chem. Phys.* **42**, 3857 (1965).

²³ M. A. Biondi and L. M. Chanin, *Phys. Rev.* **94**, 910 (1954); L. M. Chanin and M. A. Biondi, *ibid.* **106**, 473 (1957); E. C. Beaty, *ibid.* **104**, 17 (1956).